4.2.3 Terrestrial planets and satellites

4.2.3.1 Geodetic and geophysical Data

M. Grott, H. Hussmann, J. Oberst, M. Wählisch

4.2.3.1.1 Introduction

4.2.3.1.1.1 Symbols used

Table 1. List of symbols used.

Symbol	Definition	Units
a	(sub-planetary) equatorial radius	km
b	along-orbit equatorial radius	km
c	polar radius	km
d	Interval in days from standard epoch	
T	Interval in Julian centuries (356525 Julian days) from standard epoch	
W	Angle between node Q and prime meridian (Fig.1)	deg
α_0	Right ascension	deg
δ_0	Declination	deg
n	Degree of the spherical harmonic decomposition	–
m	Order of the spherical harmonic decomposition	–
U	Gravitational potential	$m^2\ s^{-2}$
G	Gravitational constant	$m^3 kg^{-1} s^{-2}$
GM	Planetocentric constant	$m^3\ s^{-2}$
r	Radial distance	m
R	Planetary radius	m
$C_{n,m}$, $S_{n,m}$	Gravitational coefficients of degree n and order m	
N_{nm}	Normalized associated Legendre functions of degree n and order m	–
P_{nm}	Associated Legendre functions of degree n and order m	–
P_n	Legendre polynomial of degree n	–
ϕ	Longitude $\in [-\pi/2,\pi/2]$ or $-90°$ to $90°$	–
θ	Latitude $\in [0,2\pi]$ or $0°$ to $360°$	–
δ_{ij}	Kronecker delta	–
J_n	Zonal gravitational coefficient	–
g_r	Radial free-air gravity anomaly	mGal
N	Geoid height	m
ω	Angular velocity	s^{-1}

4.2.3.1.1.2 Overview

Planetary coordinate systems typically are defined by the planet's rotation and location of the equator plane. They originate at the bodies' center of mass (COM). The rotational axis defines the z-axis, whereas the equator constrains the plane of the x- and y-axes. The definition of the prime meridian is not unique. In many cases, this meridian is defined by some prominent crater. However, if bodies are in locked in 1:1 commensurability between spin and orbit period, the mean sub-planet point defines the prime meridian. For the Moon, e.g., the moment-of-inertia axes can be used to define the prime meridian.

4.2.3.1.2 Rotation and shape

4.2.3.1.2.1 Rotational elements

The rotational elements describe the planetary coordinate systems with respect to an inertial system. Approximate expressions to convert planetary coordinates to the epochless International Celestial Reference Frame (ICRF) have been derived. The north pole is defined to be the pole of rotation that lies on the north side of the invariable plane of the solar system. The direction to the north pole is specified by the value of its right ascension α_0 and declination δ_0, whereas $\alpha_0 + 90°$ (one of the two intersection points of the body's equator and the ICRF equator) is defined as node Q (Fig. 1). The location of the prime meridian is specified by the angle W that is measured along the planet's equator in the easterly direction with respect to the planet's north pole from the node Q. In case of W is defined by a cartographic position, the constant in the expression $W = W_0 + \dot{W}d$ (d is the interval in days from the standard epoch) is chosen so that the ephemeris position follows the motion of the cartographic position as closely as possible. If W increases with time (i.e. $\dot{W}$ is positive), the planet has a direct (or prograde) rotation, and if W decreases with time, the rotation is said to be retrograde. In cases where sufficiently accurate tracking data are available (e.g. for the Moon and Mars), expressions for the precession of the rotational axis have been established. Bodies that show chaotic rotation, such as the small Saturnian satellite Hyperion have defied any definition of a coordinate system up to the present day.

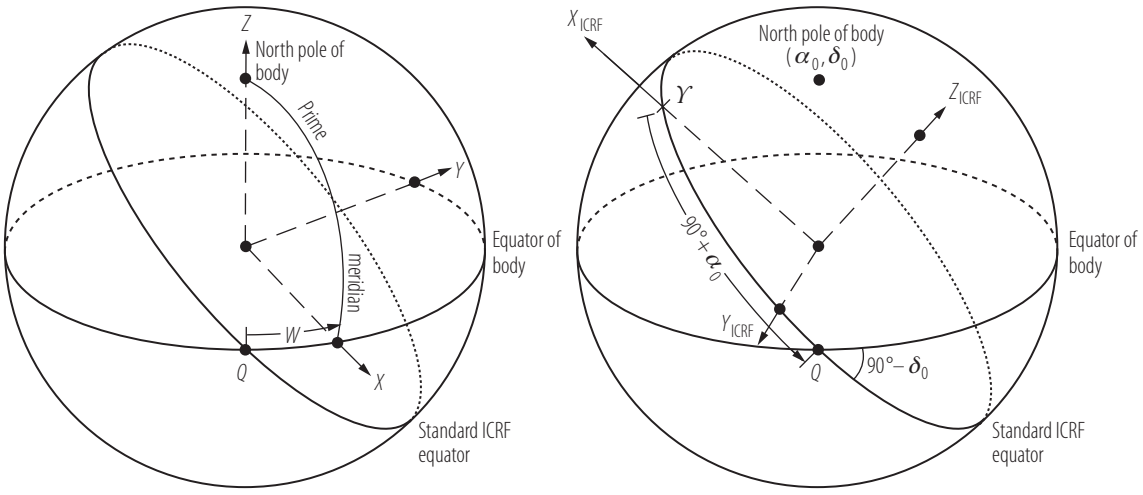

Fig. 1. The coordinate system of the planet/satellite and the reference system to define the orientation of the planet/satellite (see text for further explanation).

Table 2. Right ascension α_0, declination δ_0, and the angle W between the node Q and the prime meridian (see Fig.1) of the terrestrial planets in the ICRF [07Sei].

Mercury	$\alpha_0 = 281.^\circ01 - 0.033T$	$\delta_0 = 61.^\circ45 - 0.005T$	$W = 329.^\circ548 + 6.1385025d$
	The 20° meridian is defined by the crater Hun Kal.		
Venus	$\alpha_0 = 272.^\circ76$	$\delta_0 = 67.^\circ16$	$W = 160.^\circ20 - 1.4813688d$
	The 0° meridian is defined by the central peak in the crater Ariadne.		
Earth	$\alpha_0 = 0.^\circ00 - 0.641T$	$\delta_0 = 90.^\circ00 - 0.557T$	$W = 190.^\circ147 + 360.9856235d$
Mars	$\alpha_0 = 317.^\circ68143 - 0.1061T$	$\delta_0 = 52.^\circ88650 - 0.0609T$	$W = 176.^\circ630 + 350.89198226d$
	The 0° meridian is defined by the crater Airy-0.		

4.2.3.1.2.2 Shape

Size and shape constitute fundamental properties of any planetary body. The general shape of planets and satellites is described with respect to a reference surface. Spheres, ellipsoids ($a = b > c$ where a and b are the radii in the equatorial plane), or triaxial ellipsoids ($a \neq b \neq c$) are commonly used to describe such a reference surface. The radii are computed to fit available topographic data best. Table 4 and 5 give an overview of the size and shape parameters of the planets and satellites, respectively. The Moon and Mars are known to have pronounced offset between their centers of mass (COM) and centers of figure (COF). A highly accurate shape model is available for Mars. In Table 4 the average (AVG), north (N), and south (S) polar radii of Mars are given. It is common to approximate the reference surface of Mars by a rotational spheroid with an equatorial radius and average polar radius. In the last decades, planetary bodies were observed by an increasing number of space missions (see Section 4.2.6). As new data become available, planet rotation and shape information are frequently updated. Recommended rotation and shape data are published by the IAU (International Astronomical Union) on a regular basis [07Sei].

4.2.3.1.2.3 Method

Coordinates for any place on Earth are easily obtained from GPS readings or similar positioning systems. Such sophisticated positioning systems do not exist for the planets. Likewise, only very few surface geodetic measurements from landed spacecraft are available (see Section 4.2.6). Therefore, planetary reference systems must be realized from astronomical observations and from remote sensing observations of surface morphology, e.g. by radar measurements, imaging or Laser altimetry. Image- or planetary radii base maps, from which coordinates of morphologic features of interest can be readily extracted, and to which other data products can be co-registered may be produced by various techniques. In photogrammetry, the production of base maps is traditionally preceded by a control point network analysis. The networks consist of large catalogs of prominent landmarks (typically: small craters) for which coordinates are precisely known. Control point coordinates and their errors are determined by bundle block adjustments which involve the simultaneous inversion of large numbers of line/sample coordinates in large numbers of images. Coordinates can be determined in two dimensions (holding radius fixed) or in three dimensions. Lander stations constitute unique anchor points for the networks, as for these the coordinates in the planet-fixed coordinate system as well as coordinates in image space are typically well known. By joint analysis of lander tracking, the coordinate system of the body and its relationship to ICRF can be computed very precisely. This includes the observed location of the rotational pole, the rotational rate, parameters of precession, and the prime meridian [97Fol]. With the availability of

Table 3. Right ascension α_0, declination δ_0, and the angle W between the node Q and the prime meridian (see Fig.1) of the satellites in the ICRF [07Sei].

	α_0	δ_0	W
Earth: Moon	$269.^\circ9949$	$66.^\circ5392$	$38.^\circ3213$
	$+0.0031T$	$+0.0130T$	$+13.17635815d$
	$-3.8787 \sin E1$	$+1.5419 \cos E1$	$-1.4 \times 10^{-12} d^2$
	$-0.^\circ1204 \sin E2$	$+0.0239 \cos E2$	$+3.5610 \sin E1$
	$+0.0700 \sin E3$	$-0.0278 \cos E3$	$+0.1208 \sin E2$
	$-0.0172 \sin E4$	$+0.0068 \cos E4$	$-0.0642 \sin E3$
	$+0.0072 \sin E6$	$-0.0029 \cos E6$	$+0.0158 \sin E4$
	$-0.0052 \sin E10$	$+0.0009 \cos E7$	$+0.0252 \sin E5$
	$+0.0043 \sin E13$	$+0.0008 \cos E10$	$-0.0066 \sin E6$
		$-0.0009 \cos E13$	$-0.0047 \sin E7$
			$-0.0046 \sin E8$
			$+0.0028 \sin E9$
			$+0.0052 \sin E10$
			$+0.0040 \sin E11$
			$+0.0019 \sin E12$
			$-0.0044 \sin E13$

These formulae are precise to approximately 150 m.

where
$E1 = 125.^\circ045 - 0.^\circ0529921d$, $E2 = 250.^\circ089 - 0.^\circ1059842d$, $E3 = 260.^\circ008 + 13.^\circ0120009d$,
$E4 = 176.625 + 13.3407154d$, $E5 = 357.529 + 0.9856003d$, $E6 = 311.589 + 26.4057084d$,
$E7 = 134.963 + 13.0649930d$, $E8 = 276.617 + 0.3287146d$, $E9 = 34.226 + 1.7484877d$,
$E10 = 15.134 - 0.1589763d$, $E11 = 119.743 + 0.0036096d$, $E12 = 239.961 + 0.1643573d$,
$E13 = 25.053 + 12.9590088d$

		α_0	δ_0	W
Mars:	Phobos	$317.^\circ68$	$52.^\circ90$	$35.^\circ06$
		$-0.108T$	$-0.061T$	$+1128.8445850d$
		$+1.79 \sin M1$	$-1.08 \cos M1$	$+8.864T^2$
				$-1.42 \sin M1$
				$-0.78 \sin M2$
	Deimos	$316.^\circ65$	$53.^\circ52$	$79.^\circ41$
		$-0.108T$	$-0.061T$	$+285.1618970d$
		$+2.98 \sin M3$	$-1.78 \cos M3$	$-0.520T^2$
				$-2.58 \sin M3$
				$+0.19 \cos M3$

where
$M1 = 169.^\circ51 - 0.^\circ4357640d$, $M2 = 192.^\circ93 + 1128.^\circ4096700d + 8.^\circ864T^2$,
$M3 = 53.^\circ47 - 0.^\circ0181510d$

Table 3. Right ascension α_0, declination δ_0, and the angle W between the node Q and the prime meridian (see Fig.1) of the satellites in the ICRF [07Sei].

		α_0	δ_0	W
Jupiter:	Metis	$268.^\circ05$	$64.^\circ49$	$346.^\circ09$
		$-0.009T$	$+0.003T$	$+1221.2547301d$
	Adrastea	$268.^\circ05$	$64.^\circ49$	$33.^\circ29$
		$-0.009T$	$+0.003T$	$+1206.9986602d$
	Amalthea	$268.^\circ05$	$64.^\circ49$	$231.^\circ67$
		$-0.009T$	$+0.003T$	$+722.6314560d$
		$-0.84\sin J1$	$-0.36\cos J1$	$+0.76\sin J1$
		$+0.01\sin 2J1$		$-0.01\sin 2J1$
	Thebe	$268.^\circ05$	$64.^\circ49$	$8.^\circ56$
		$-0.009T$	$+0.003T$	$+533.7004100d$
		$-2.11\sin J2$	$-0.91\cos J2$	$+1.91\sin J2$
		$+0.04\sin 2J2$	$+0.01\cos 2J2$	$-0.04\sin 2J2$
	Io	$268.^\circ05$	$64.^\circ50$	$200.^\circ39$
		$-0.009T$	$+0.003T$	$+203.4889538d$
		$+0.094\sin J3$	$+0.040\cos J3$	$-0.085\sin J3$
		$+0.024\sin J4$	$+0.011\cos J4$	$-0.022\sin J4$
	Europa	$268.^\circ08$	$64.^\circ51$	$36.^\circ022$
		$-0.009T$	$+0.003T$	$+101.3747235d$
		$+1.086\sin J4$	$+0.468\cos J4$	$-0.980\sin J4$
		$+0.060\sin J5$	$+0.026\cos J5$	$-0.054\sin J5$
		$+0.015\sin J6$	$+0.007\cos J6$	$-0.014\sin J6$
		$+0.009\sin J7$	$+0.002\cos J7$	$-0.008\sin J7$
		The 182° meridian is defined by the crater Cilix.		
	Ganymede	$268.^\circ20$	$64.^\circ57$	$44.^\circ064$
		$-0.009T$	$+0.003T$	$+50.3176081d$
		$-0.037\sin J4$	$-0.016\cos J4$	$+0.033\sin J4$
		$+0.431\sin J5$	$+0.186\cos J5$	$-0.389\sin J5$
		$+0.091\sin J6$	$+0.039\cos J6$	$-0.082\sin J6$
		The 128° meridian is defined by the crater Anat.		
	Callisto	$268.^\circ72$	$64.^\circ83$	$259.^\circ51$
		$-0.009T$	$+0.003T$	$+21.5710715d$
		$-0.068\sin J5$	$-0.029\cos J5$	$+0.061\sin J5$
		$+0.590\sin J6$	$+0.254\cos J6$	$-0.533\sin J6$
		$+0.010\sin J8$	$-0.004\cos J8$	$-0.009\sin J8$
		The 326° meridian is defined by the crater Saga.		

where

$J1 = 73.^\circ32 + 91472.^\circ9T$, $J2 = 24.^\circ62 + 45137.^\circ2T$, $J3 = 283.^\circ90 + 4850.^\circ7T$,
$J4 = 355.80 + 1191.3T$, $J5 = 119.90 + 262.1T$, $J6 = 229.80 + 64.3T$,
$J7 = 352.25 + 2382.6T$, $J8 = 113.35 + 6070.0T$

Table 3. Right ascension α_0, declination δ_0, and the angle W between the node Q and the prime meridian (see Fig.1) of the satellites in the ICRF [07Sei].

		α_0	δ_0	W
Saturn:	Pan	$40\overset{\circ}{.}6$	$83\overset{\circ}{.}5$	$48\overset{\circ}{.}8$
		$-0.036T$	$-0.004T$	$+626.0440000d$
	Atlas	$40\overset{\circ}{.}58$	$83\overset{\circ}{.}53$	$137\overset{\circ}{.}88$
		$-0.036T$	$-0.004T$	$+598.3060000d$
	Prometheus	$40\overset{\circ}{.}58$	$83\overset{\circ}{.}53$	$296\overset{\circ}{.}14$
		$-0.036T$	$-0.004T$	$+587.289000d$
	Pandora	$40\overset{\circ}{.}58$	$83\overset{\circ}{.}53$	$162\overset{\circ}{.}92$
		$-0.036T$	$-0.004T$	$+572.7891000d$
	Epimetheus*	$40\overset{\circ}{.}58$	$83\overset{\circ}{.}52$	$293\overset{\circ}{.}87$
		$-0.036T$	$-0.004T$	$+518.4907239d$
		$-3.153\sin S1$	$-0.356\cos S1$	$+3.133\sin S1$
		$+0.086\sin 2S1$	$+0.005\cos 2S1$	$-0.086\sin 2S1$
	Janus*	$40\overset{\circ}{.}58$	$83\overset{\circ}{.}52$	$58\overset{\circ}{.}83$
		$-0.036T$	$-0.004T$	$+518.2359876d$
		$-1.623\sin S2$	$-0.183\cos S2$	$+1.613\sin S2$
		$+0.023\sin 2S2$	$+0.001\cos 2S2$	$-0.023\sin 2S2$
	Mimas	$40\overset{\circ}{.}66$	$83\overset{\circ}{.}52$	$337\overset{\circ}{.}46$
		$-0.036T$	$-0.004T$	$+381.9945550d$
		$+13.56\sin S3$	$-1.53\cos S3$	$-13.48\sin S3$
				$-44.85\sin S5$
		The 162° meridian is defined by the crater Palomides.		
	Enceladus	$40\overset{\circ}{.}66$	$83\overset{\circ}{.}52$	$2\overset{\circ}{.}82$
		$-0.036T$	$-0.004T$	$+262.7318996d$
		The 5° meridian is defined by the crater Salih.		
	Tethys	$40\overset{\circ}{.}66$	$83\overset{\circ}{.}52$	$10\overset{\circ}{.}45$
		$-0.036T$	$-0.004T$	$+190.6979085d$
		$+9.66\sin S4$	$-1.09\cos S4$	$-9.60\sin S4$
				$2.23\sin S5$
		The 299° meridian is defined by the crater Arete.		
	Telesto*	$50\overset{\circ}{.}51$	$84\overset{\circ}{.}06$	$56\overset{\circ}{.}88$
		$-0.036T$	$-0.004T$	$+190.6979332d$
	Calypso*	$36\overset{\circ}{.}41$	$85\overset{\circ}{.}04$	$153\overset{\circ}{.}51$
		-0.036	$-0.004T$	$+190.6742373d$
	Dione	$40\overset{\circ}{.}66$	$83\overset{\circ}{.}52$	$357\overset{\circ}{.}00$
		-0.036	$-0.004T$	$+131.5349316d$
		The 63° meridian is defined by the crater Palinurus.		
	Helene	$40\overset{\circ}{.}85$	$83\overset{\circ}{.}34$	$245\overset{\circ}{.}12$
		$-0.036T$	$-0.004T$	$+131.6174056d$
	Rhea	$40\overset{\circ}{.}38$	$83\overset{\circ}{.}55$	$235\overset{\circ}{.}16$
		$-0.036T$	$-0.004T$	$+79.6900478d$
		$+3.10\sin S6$	$-0.35\cos S6$	$-3.08\sin S6$
		The 340° meridian is defined by the crater Tore.		

* These expressions are valid for the period of the Voyager encounters. Because of precession they may not be accurate at other time periods.

Table 3. Right ascension α_0, declination δ_0, and the angle W between the node Q and the prime meridian (see Fig.1) of the satellites in the ICRF [07Sei].

	Titan	$36.^\circ41$	$83.^\circ94$	$189.^\circ64$
		$-0.036T$	$-0.004T$	$+22.5769768d$
		$+2.66\sin S7$	$-0.30\cos S7$	$-2.64\sin S7$
	Iapetus	$318.^\circ16$	$75.^\circ03$	$350.^\circ20$
		$-3.949T$	$-1.143T$	$+4.5379572d$
		The 276° meridian is defined by the crater Almeric.		
	Phoebe	$356.^\circ90$	$77.^\circ80$	$178.^\circ58$
				$+931.639d$

where

$S1 = 353.^\circ32 + 75706.^\circ7T$, $S2 = 28.^\circ72 + 75706.^\circ7T$, $S3 = 177.^\circ40 - 36505.^\circ5T$
$S4 = 300.00 - 7225.9T$, $S5 = 316.45 + 506.2T$, $S6 = 345.20 - 1016.3T$,
$S7 = 29.80 - 52.1T$

		α_0	δ_0	W
Uranus:	Cordelia	$257.^\circ31$	$-15.^\circ18$	$127.^\circ69$
		$-0.15\sin U1$	$+0.14\cos U1$	$-1074.5205730d$
				$-0.04\sin U1$
	Ophelia	$257.^\circ31$	$-15.^\circ18$	$130.^\circ35$
		$-0.09\sin U2$	$+0.09\cos U2$	$-956.4068150d$
				$-0.03\sin U2$
	Bianca	$257.^\circ31$	$-15.^\circ18$	$105.^\circ46$
		$-0.16\sin U3$	$+0.16\cos U3$	$-828.3914760d$
				$-0.04\sin U3$
	Cressida	$257.^\circ31$	$-15.^\circ18$	$59.^\circ16$
		$-0.04\sin U4$	$+0.04\cos U4$	$-776.5816320d$
				$-0.01\sin U4$
	Desdemona	$257.^\circ31$	$-15.^\circ18$	$95.^\circ08$
		$-0.17\sin U5$	$+0.16\cos U5$	$-760.0531690d$
				$-0.04\sin U5$
	Juliet	$257.^\circ31$	$-15.^\circ18$	$302.^\circ56$
		$-0.06\sin U6$	$+0.06\cos U6$	$-730.^\circ1253660d$
				$-0.02\sin U6$
	Portia	$257.^\circ31$	$-15.^\circ18$	$25.^\circ03$
		$-0.09\sin U7$	$+0.09\cos U7$	$-701.4865870d$
				$-0.02\sin U7$
	Rosalind	$257.^\circ31$	$-15.^\circ18$	$314.^\circ90$
		$-0.29\sin U8$	$+0.28\cos U8$	$-644.6311260d$
				$-0.08\sin U8$
	Belinda	$257.^\circ31$	$-15.^\circ18$	$297.^\circ46$
		$-0.03\sin U9$	$+0.03\cos U9$	$-577.3628170d$
				$-0.01\sin U9$
	Puck	$257.^\circ31$	$-15.^\circ18$	$91.^\circ24$
		$-0.33\sin U10$	$+0.31\cos U10$	$-472.5450690d$
				$-0.09\sin U10$

Table 3. Right ascension α_0, declination δ_0, and the angle W between the node Q and the prime meridian (see Fig.1) of the satellites in the ICRF [07Sei].

	Miranda	$257.^\circ 43$	$-15.^\circ 08$	$30.^\circ 70$
		$+4.41 \sin U11$	$+4.25 \cos U11$	$-254.6906892d$
		$-0.04 \sin 2U11$	$-0.02 \cos 2U11$	$-1.27 \sin U12$
				$+0.15 \sin 2U12$
				$+1.15 \sin U11$
				$-0.09 \sin 2U11$
	Ariel	$257.^\circ 43$	$-15.^\circ 10$	$156.^\circ 22$
		$+0.29 \sin U13$	$+0.28 \cos U13$	$-142.8356681d$
				$+0.05 \sin U12$
				$0.08 \sin U13$
	Umbriel	$257.^\circ 43$	$-15.^\circ 10$	$108.^\circ 05$
		$+0.21 \sin U14$	$+0.20 \cos U14$	$-86.8688923d$
				$-0.09 \sin U12$
				$+0.06 \sin U14$
	Titania	$257.^\circ 43$	$-15.^\circ 10$	$77.^\circ 74$
		$+0.29 \sin U15$	$+0.28 \cos U15$	$-41.3514316d$
				$+0.08 \sin U15$
	Oberon	$257.^\circ 43$	$-15.^\circ 10$	$6.^\circ 77$
		$+0.16 \sin U16$	$+0.16 \cos U16$	$-26.7394932d$
				$+0.04 \sin U16$

where

$U1 = 115.^\circ 75 + 54991.^\circ 87T$, $U2 = 141.^\circ 69 + 41887.^\circ 66T$, $U3 = 135.^\circ 03 + 29927.^\circ 35T$,
$U4 = 61.77 + 25733.59T$, $U5 = 249.32 + 24471.46T$, $U6 = 43.86 + 22278.41T$,
$U7 = 77.66 + 20289.42T$, $U8 = 157.36 + 16652.76T$, $U9 = 101.81 + 12872.63T$,
$U10 = 138.64 + 8061.81T$, $U11 = 102.23 - 2024.22T$, $U12 = 316.41 + 2863.96T$,
$U13 = 304.01 - 51.94T$, $U14 = 308.71 - 93.17T$, $U15 = 340.82 - 75.32T$,
$U16 = 259.14 - 504.81T$

		α_0	δ_0	W
Neptune	Naiad	$299.^\circ 36$	$43.^\circ 36$	$254.^\circ 06$
		$+0.70 \sin N$	$-0.51 \cos N$	$+1222.8441209$d
		$-6.49 \sin N1$	$-4.75 \cos N1$	$-0.48 \sin N$
		$+0.25 \sin 2N1$	$+0.09 \cos 2N1$	$+4.40 \sin N1$
				$-0.27 \sin 2N1$
	Thalassa	$299.^\circ 36$	$43.^\circ 45$	$102.^\circ 06$
		$+0.70 \sin N$	$-0.51 \cos N$	$+1155.7555612d$
		$-0.28 \sin N2$	$-0.21 \cos N2$	$-0.48 \sin N$
				$+0.19 \sin N2$
	Despina	$299.^\circ 36$	$43.^\circ 45$	$306.^\circ 51$
		$+0.70 \sin N$	$-0.51 \cos N$	$+1075.7341562$d
		$-0.09 \sin N3$	$-0.07 \cos N3$	$-0.49 \sin N$
				$+0.06 \sin N3$
	Galatea	$299.^\circ 36$	$43.^\circ 43$	$258.^\circ 09$
		$+0.70 \sin N$	$-0.51 \cos N$	$+839.6597686$d
		$-0.07 \sin N4$	$-0.05 \cos N4$	$-0.48 \sin N$
				$+0.05 \sin N4$

Table 3. Right ascension α_0, declination δ_0, and the angle W between the node Q and the prime meridian (see Fig.1) of the satellites in the ICRF [07Sei].

Larissa	$299.^\circ36$	$43.^\circ41$	$179.^\circ41$
	$+0.70\sin N$	$-0.51\cos N$	$+649.0534470$d
	$-0.27\sin N5$	$-0.20\cos N5$	$-0.48\sin N$
			$+0.19\sin N5$
Proteus	$299.^\circ27$	$42.^\circ91$	$93.^\circ38$
	$+0.70\sin N$	$-0.51\cos N$	$+320.7654228$d
	$-0.05\sin N6$	$-0.04\cos N6$	$-0.48\sin N$
			$+0.04\sin N6$
Triton	$299.^\circ36$	$41.^\circ17$	$296.^\circ53$
	$-32.35\sin N7$	$+22.55\cos N7$	$-61.2572637d$
	$-6.28\sin 2N7$	$+2.10\cos 2N7$	$+22.25\sin N7$
	$-2.08\sin 3N7$	$+0.55\cos 3N7$	$+6.73\sin 2N7$
	$-0.74\sin 4N7$	$+0.16\cos 4N7$	$+2.05\sin 3N7$
	$-0.28\sin 5N7$	$+0.05\cos 5N7$	$+0.74\sin 4N7$
	$-0.11\sin 6N7$	$+0.02\cos 6N7$	$+0.28\sin 5N7$
	$-0.07\sin 7N7$	$+0.01\cos 7N7$	$+0.11\sin 6N7$
	$-0.02\sin 8N7$		$+0.05\sin 7N7$
	$-0.01\sin 9N7$		$+0.02\sin 8N7$
			$+0.01\sin 9N7$

where

$N = 357.^\circ85 + 52.^\circ316T$, $N1 = 323.^\circ92 + 62606.^\circ6T$, $N2 = 220.^\circ51 + 55064.^\circ2T$,
$N3 = 354.27 + 46564.5T$, $N4 = 75.31 + 26109.4T$, $N5 = 35.36 + 14325.4T$,
$N6 = 142.61 + 2824.6T$, $N7 = 177.85 + 52.316T$

Table 4. Size and shape parameters of the terrestrial planets [07Sei].

Planet	Mean radius [km]	Equatorial radius [km]	Polar radius [km]	RMS deviation from spheroid [km]
Mercury	2439.7 ± 1.0	same	same	1
Venus	6051.8 ± 1.0	same	same	1
Earth	6371.00 ± 0.01	6378.14 ± 0.01	6356.75 ± 0.01	3.57
Mars	3389.50 ± 0.2	3396.19 ± 0.1	AVG 3376.20 ± 0.1 N 3373.19 ± 0.1 S 3379.21 ± 0.1	3.0

reliable navigation data, base maps are often computed relying on known spacecraft position and pointing data, as well as on previously derived rotation parameters of the planet. In addition, it became popular to use the planet limb position to improve the camera pointing data [06Roa]. The highest radial topographic accuracy and good horizontal position accuracy give global planetary radii base maps, derived from multiple laser altimeter measurements. Laser track crossover analysis are applied for orbit data verification and improvement [01Neu]. Figure 2 shows the known planetary radii models of Venus, Mars, and the Moon. The Venus near-global planetary radii model was derived from radar data obtained during the Magellan mission (see Section 4.2.6) with

Table 5. Size and shape parameters for the satellites [07Sei].

Planet	Satellite	Mean radius [km]	Subplanetary equatorial radius [km]	Along orbit equatorial radius [km]	Polar radius [km]
Earth	Moon	1737.4 ± 1	1737.4 ± 1	1737.4 ± 1	1737.4 ± 1
Mars	Phobos	11.1 ± 0.15	13.4	11.2	9.2
	Deimos	6.2 ± 0.18	7.5	6.1	5.2
Jupiter	Metis	21.5 ± 4	30		20
	Adrastea	8.2 ± 4	10	8	7
	Amalthea	83.5 ± 3	125	73	64
	Thebe	49.3 ± 4	58	49	42
	Io	1821.46	1829.4	1819.3	1815.7
	Europa	1562.09	1564.13	1561.23	1560.93
	Ganymede	2632.345	2632.4	2632.29	2632.35
	Callisto	2409.3	2409.4	2409.2	2409.3
Saturn	Atlas	16 ± 4	18.5	17.2	13.5
	Prometheus	50.1 ± 3	74.0	50.0	34.0
	Pandora	41.9 ± 2	55.0	44.0	31.0
	Epimetheus	59.5 ± 3	69.0	55.0	55.0
	Janus	88.8 ± 4	97.0	95.0	77.0
	Mimas	198.2 ± 0.5	207.4 ± 0.7	196.8 ± 0.6	190.6 ± 0.3
	Enceladus	252.1 ± 0.2	256.6 ± 0.6	251.4 ± 0.2	248.3 ± 0.2
	Tethys	$533.0 \pm 1.$	540.4 ± 0.8	531.1 ± 2.6	527.5 ± 2.0
	Telesto	11 ± 4	15 ± 2.5	12.5 ± 5	7.5 ± 2.5
	Calypso	9.5 ± 4	15.0	8.0	8.0
	Dione	561.7 ± 0.9	563.8 ± 0.9	561.0 ± 1.3	560.3 ± 1.3
	Helene	16 ± 0.7	17.5 ± 2.5		
	Rhea	764.3 ± 1.8	767.2 ± 2.2	762.5 ± 0.8	763.1 ± 1.1
	Titan	2575 ± 2	2575 ± 2	2575 ± 2	2575 ± 2
	Hyperion	133 ± 8	164 ± 8	130 ± 8	107 ± 8
	Iapetus	735.6 ± 3.0	747.4 ± 3.1	747.4 ± 3.1	712.4 ± 2.0
	Phoebe	106.7 ± 1	108.6 ± 1	107.7 ± 1	101.5 ± 1
Uranus	Miranda	235.8 ± 0.7	240.4 ± 0.6	234.2 ± 0.9	232.9 ± 1.2
	Ariel	578.9 ± 0.6	581.1 ± 0.9	577.9 ± 0.6	577.7 ± 1.0
	Umbriel	584.7 ± 2.8	584.7 ± 2.8	584.7 ± 2.8	584.7 ± 2.8
	Titania	788.9 ± 1.8	788.9 ± 1.8	788.9 ± 1.8	788.9 ± 1.8
	Oberon	761.4 ± 2.6	761.4 ± 2.6	761.4 ± 2.6	761.4 ± 2.6
Neptune	Larissa	96 ± 7	104		89
	Proteus	208 ± 8	218	208	201

50 km spatial and 100 m vertical resolution. Note the gaps in the data for the high northern and southern latitudes. The coordinate system for the Moon is realized by a global network of control points, the Unified Lunar Control Network (ULCN) 2005 [06Arc]. It is mostly based on Clementine image data [94Noz] as well as laser altimetry [94Zub]. The network has on average a few hundred meter vertical and 100 m to few km horizontal absolute accuracy [06Arc]. The Mars Orbiter Laser Altimeter (MOLA) on Mars Global Surveyor (see Section 4.2.6) successfully accomplished about 600 million range measurements, from which radial topographic accuracy of 1 m and horizontal position accuracy better than 100 m have been achieved [01Neu]. Of the planets shown, Mars is

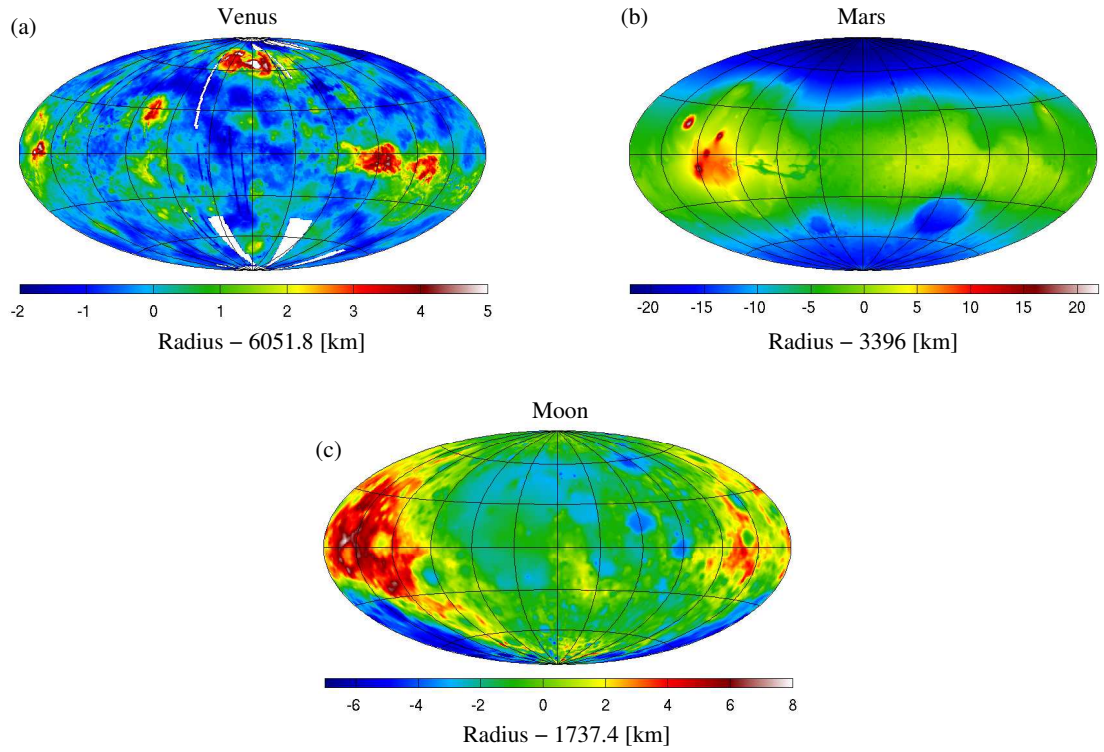

Fig. 2. (see color-picture part, page 618) Planetary radii models of Venus, Mars and the Moon. All images are in a Hammer projection with a central meridian of 0° W. The values are referenced to a sphere of radius 6051.8, 3396 and 1737.4 km for Venus, Mars and the Moon, respectively. Note the data gaps for Venus and the rotational flattening present for Mars.

the only one that exhibits a significant amount of rotational flattening.

4.2.3.1.3 Gravity studies

4.2.3.1.3.1 Method

The gravity field of a planet can be derived from Doppler tracking of orbiting or passing spacecraft. The frequency shifts of radio signals transmitted from the Earth to the probe and back is inverted to give the acceleration in the direction of the line of sight. The gravity field of the planet is then derived from a multitude of these measurements.
For the terrestrial planets, gravity models have been constructed using radio tracking data from a variety of space missions. The most recent gravity models rely on tracking data from the Grace and Lageos missions for the Earth [08För], the Pioneer Venus Orbiter and Magellan for Venus [06Rap], Mars Global Surveyor, Mars Odyssey, Mars Pathfinder and the Viking Lander 1 for Mars [05Tyl], and Lunar Orbiters 1 to 5, the Apollo 15 and 16 subsatellites, and the Clementine and Lunar Prospector missions for the Moon [99Kon2]. Current gravity models for the terrestrial planets are summarized in Table 6.

Table 6. Current gravity models of the Earth, Venus, Mars and the Moon. Resolution is given in terms of degree n and order m of the spherical harmonic decomposition.

Planet	Name	Resolution	References
Earth	EIGEN-GL04C	$n, m = 360$	[08För]
Venus	SHGJ180	$n, m = 180$	[06Rap, 99Kon1]
Mars	MGS95J	$n, m = 95$	[05Tyl, 06Kon]
Moon	LP165P	$n, m = 165$	[97Lem, 99Kon2, 01Kon]

4.2.3.1.3.2 Gravity Field Coefficients

Several large scale physical properties of the planets can be derived from harmonic expansions of their gravity fields. The corresponding external gravitational potential U at latitude $\theta \in [-\pi/2, \pi/2]$, longitude $\phi \in [0, 2\pi]$ and distance r (with r larger than the planetary radius R_p) can be represented as

$$U(r,\theta,\phi) = \frac{GM}{r}\sum_{n=0}^{\infty}\sum_{m=0}^{n}\left(\frac{R_p}{r}\right)^n (C_{nm}\cos(m\phi) + S_{nm}\sin(m\phi))N_{nm}(\cos\theta) \quad (1)$$

where the normalized associated Legendre functions are given by

$$N_{nm}(x) = \sqrt{(2-\delta_{0m})(2n+1)\frac{(n-m)!}{(n+m)!}}P_{nm}(x) \quad (2)$$

and

$$P_{nm}(x) = (1-x^2)^{m/2}\frac{d^m}{dx^m}P_n(x) \quad (3)$$

$$P_n(x) = \frac{1}{2^n n!}\frac{d^n}{dx^n}(x^2-1)^n \quad (4)$$

The usual convention for the representation of the zonal coefficients is

$$J_n = -C_{n0} \quad (5)$$

In particular, J_2 measures the planet's oblateness and J_3 the asymmetry between the northern and southern hemispheres. Low order coefficients C_{nm} and S_{nm} of the gravity fields of the Earth, Venus, Mars and the Moon are given in Table 7.

4.2.3.1.3.3 Gravity studies of the Earth, Venus, Mars and the Moon

The radial free-air gravity anomaly g_r can be calculated from the spherical harmonic decomposition of the gravity field by

$$g_r(r) = \frac{GM}{r^2}\sum_{n=0}^{\infty}\sum_{m=0}^{n}\left(\frac{R_p}{r}\right)^n (n+1)(C_{nm}\cos(m\phi) + S_{nm}\sin(m\phi))N_{nm}(\cos\theta) \quad (6)$$

The geoid is defined by a specific equipotential surface and the height N of the geoid with respect to a best-fitting spherical reference surface of radius R_p can be approximated to first order by [07Wie]

$$N(r,\theta,\phi) = r\sum_{n=2}^{\infty}\sum_{m=0}^{n}\left(\frac{R_p}{r}\right)^n (C_{nm}\cos(m\phi) + S_{nm}\sin(m\phi))N_{nm}(\cos\theta) - \frac{\omega^2 r^4}{3\sqrt{5}GM}N_{20} \quad (7)$$

where ω is the angular velocity of the rotating planet.

Table 7. Gravity field coefficients to degree n and order m of 4 for the Earth, Venus, Mars and the Moon. The gravitational acceleration GM and reference radius R_p for the particular models are also given. ω is the angular velocity necessary for the calculation of the geoid.

		Earth		Venus	
n	m	$C_{nm} \times 10^9$	$S_{nm} \times 10^9$	$C_{nm} \times 10^9$	$S_{nm} \times 10^9$
2	0	-484165.227 ± 0.025	0	-1969.72 ± 0.67	0
2	1	-0.255 ± 0.016	1.440 ± 0.016	26.80 ± 0.34	13.24 ± 0.36
2	2	2439.364 ± 0.017	-1400.285 ± 0.017	857.77 ± 0.97	-95.53 ± 0.91
3	0	957.205 ± 0.010	0	796.82 ± 0.26	0
3	1	2030.454 ± 0.015	248.204 ± 0.015	2348.30 ± 0.28	541.62 ± 0.27
3	2	904.781 ± 0.019	-618.986 ± 0.019	-8.53 ± 0.40	809.06 ± 0.42
3	3	721.282 ± 0.024	1414.378 ± 0.024	-188.01 ± 0.61	213.48 ± 0.62
4	0	539.992 ± 0.004	0	715.80 ± 0.20	0
4	1	-536.143 ± 0.004	$-.473.563 \pm 0.004$	-457.42 ± 0.20	491.60 ± 0.20
4	2	350.504 ± 0.006	662.477 ± 0.006	126.32 ± 0.18	483.57 ± 0.16
4	3	990.862 ± 0.009	$-.200.957 \pm 0.009$	-174.66 ± 0.21	-116.49 ± 0.19
4	4	-188.494 ± 0.009	308.822 ± 0.010	172.51 ± 0.62	1376.61 ± 0.51
		GM [km^3 s^{-2}]	398600.4415		324858.5920
		R_p [km]	6378.13		6051
		$\omega \times 10^6$[rad s^{-1}]	72.92115 [1])		-0.299.24 [1])

		Mars		Moon	
n	m	$C_{nm} \times 10^9$	$S_{nm} \times 10^9$	$C_{nm} \times 10^9$	$S_{nm} \times 10^9$
2	0	-875021.446 ± 0.022	0	-90890.18 ± 5.46	0
2	1	0.240 ± 0.012	0.228 ± 0.012	-2.72 ± 4.50	-0.75 ± 3.48
2	2	-84635.831 ± 0.006	48934.512 ± 0.008	34635.49 ± 3.68	16.72 ± 3.04
3	0	-11896.460 ± 0.018	0	-3203.59 ± 6.48	0
3	1	3803.574 ± 0.012	25177.363 ± 0.012	26327.44 ± 7.49	5464.36 ± 4.46
3	2	-15947.887 ± 0.010	8361.380 ± 0.010	14188.17 ± 6.74	4892.03 ± 6.03
3	3	35054.079 ± 0.007	25574.349 ± 0.007	12286.05 ± 4.51	-1785.44 ± 4.56
4	0	5128.584 ± 0.019	0	3197.30 ± 7.22	0
4	1	4216.387 ± 0.017	3763.285 ± 0.017	-5996.60 ± 9.01	1661.93 ± 5.46
4	2	-952.535 ± 0.013	-8980.866 ± 0.013	-7081.80 ± 9.99	-6783.62 ± 8.97
4	3	6456.813 ± 0.009	-193.214 ± 0.009	-1362.29 ± 8.76	-13443.47 ± 8.73
4	4	309.733 ± 0.005	-12873.020 ± 0.005	-6025.77 ± 6.28	3939.63 ± 5.36
		GM [km^3 s^{-2}]	42828.375214		4902.01056
		R_p [km]	3396		1738
		$\omega \times 10^6$ [rad s^{-1}]	70.8821820 [2])		2.6617073 [1])

[1]) [95Yod]
[2]) [01Yua]

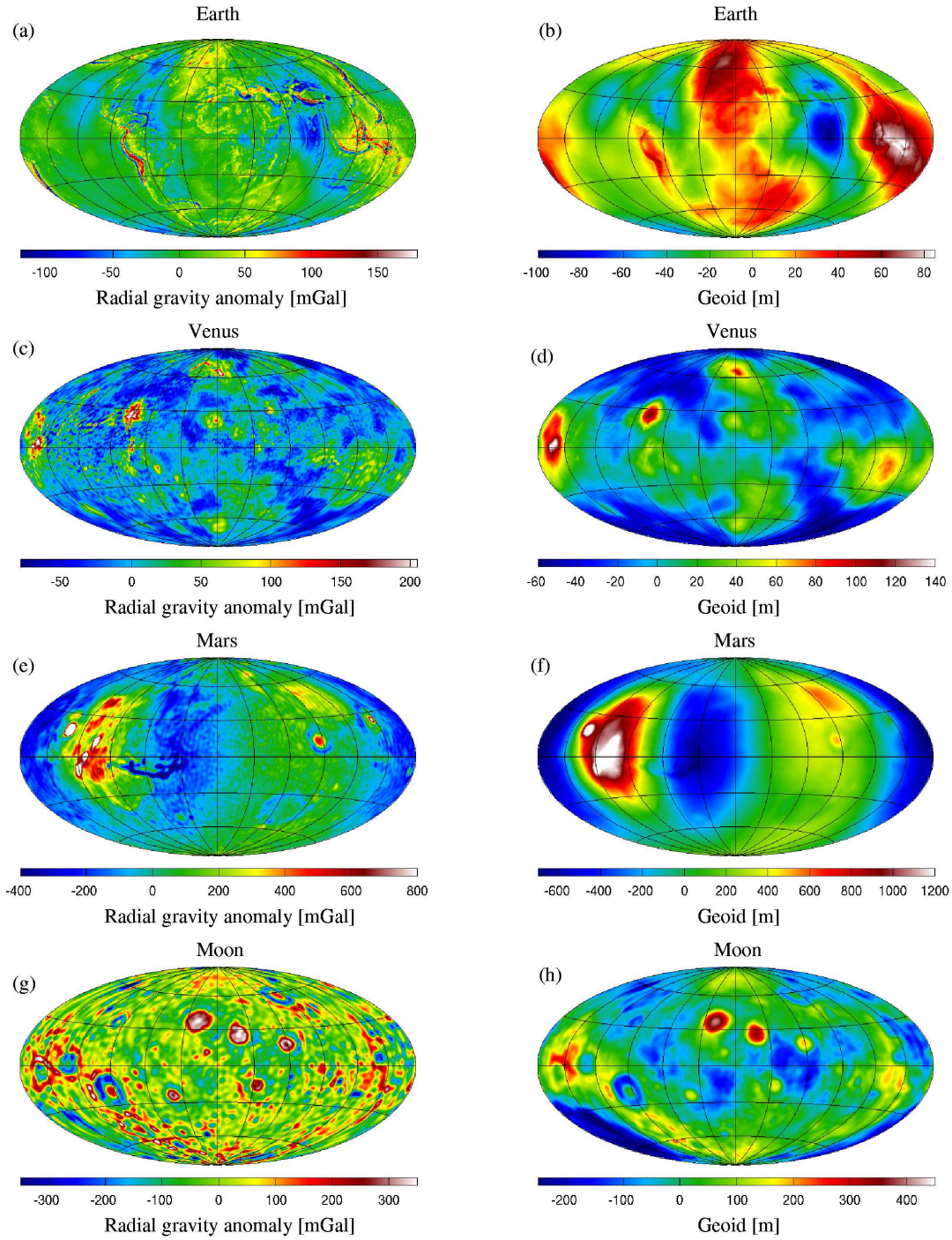

Fig. 3. (see color-picture part, page 619) Radial gravity anomaly g_r and geoid height N for the Earth, Venus, Mars and the Moon. All images are in a Hammer projection with a central meridian of 0° W. (a)-(b) g_r and N for the Earth, evaluating the model EIGEN-GL04C [08För] at a reference radius $R_\mathrm{p} = 6378.13$ km and setting the zonal degree-2 term C_{20} to zero. (c)-(d) g_r and N for Venus, evaluating the model SHGJ180 [06Rap] at $R_\mathrm{p} = 6051$ km. (e)-(f) g_r and N for Mars, evaluating the model MGS95J [05Tyl] at $R_\mathrm{p} = 3396$ km and setting the zonal degree-2 term C_{20} to zero. (g)-(h) g_r and N for the Moon, evaluating the model LP165P [97Lem] at $R_\mathrm{p} = 1738$ km and setting the zonal degree-2 terms C_{20} and C_{22} to zero.

The radial gravity anomaly g_r and geoid height N for the Earth, Venus, Mars and the Moon are shown in Figure 3. As the gravity fields of the Earth, Mars and the Moon are dominated by the degree 2 zonal term C_{20}, this term has been set to zero for plotting purposes. Additionally, the C_{22} term has been set to zero for the Moon. The geoid height N shown in Fig. 3 has been evaluated for the same parameters, neglecting the rotational flattening term in Eq. 7, which dominates the geoids of Earth and Mars.

On the Earth, the largest gravity anomalies (Fig. 3a) are associated with topography such as trenches and seamounts, and the geoid (Fig. 3b) shows relatively small undulation of only 200 m. This picture is similar for the gravity anomalies of Venus (Fig. 3c), which are also highly correlated with surface topography. The largest anomalies of 200-300 mGal are associated with the volcanoes Maat and Ozza Montes and the high-standing topography of Maxwell Montes and Beta Regio. Similar to the Earth, geoid undulations (Fig. 3d) are of the order of only 200 m [99Kon1].

For Mars, large radial gravity anomalies (Fig. 3e) are associated with the volcanoes of the Tharsis rise. Also, large impact basins such as Isidis, Argyre and Utopia show positive anomalies. Negative anomalies surround Tharsis [01Phi], Valles Marineris and some mountains and volcanoes. The geoid anomalies of Mars (Fig. 3f) are the largest among the terrestrial planets, with values spanning –600 to 1200 m.

The major features of the lunar gravity field (Fig. 3g) are large positive anomalies which are associated with the nearside impact basins [07Wie]. These are usually referred to as mascons ('mass concentrations', e.g. [68Mul]) and exhibit anomalies of a few hundred mGal. Furthermore, some of these basins are surrounded by concentric gravity lows. The lunar geoid (Fig. 3e) shows undulations in excess of 500 m [01Kon].

4.2.3.1.4 Topography

Because planets and satellites other than the Earth have no sea level, their datum for topography (the zero elevation) is defined as a sphere, a two-axial spheroid or – if known – a gravitational equipotential surface. For Venus, this reference surface is given by a sphere of 6051.8 km radius. For Mars it is given as the gravitational equipotential surface whose average radius at the equator is equal to the mean equatorial radius of 3396 km. For the Moon, the elevation reference is a spheroid with an equatorial radius of 1737.4 km and a flattening of 1/3234.93. The reference surface for the Earth is the mean sea level, as given by the WGS84 EGM96 geoid.

Recent topographic models for the Earth, Venus, Mars and the Moon are summarized in Table 8 and topographic maps derived from these models are shown in Fig. 4. For the Earth, the distribution of elevations is bimodal and the two sharp peaks in the hypsometric curve (Fig. 5a) represent the level of the continental shelfs and the deep ocean floor, respectively. The topography of Venus is characterized by its low elevation planes, 'continental' plateaus and volcanic swells, and the distribution of elevations is sharply unimodal (Fig. 5b). Mars (Fig. 5c) topography is characterized by the dichotomy between the northern lowlands and southern highland terrains, as represented by the peaks around –4 and 1.5 km in the hypsometric curve (Fig. 5c), respectively. The small peak at –7 km is connected to the Hellas impact basin. The lunar topography is dominated by the elevation difference between the low-standing nearside and high-standing farside topography as well as the giant farside South Pole-Aitken impact basin. The distribution of elevations on the Moon is unimodal (Fig. 5d), but less sharply peaked than that of Venus.

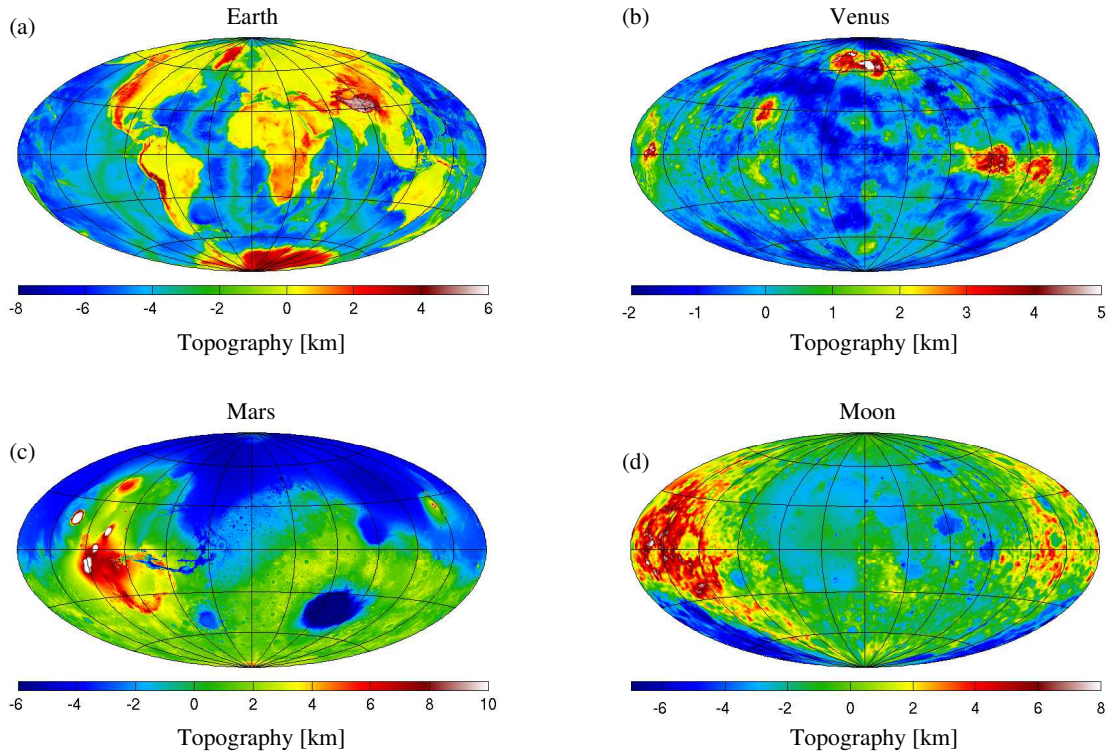

Fig. 4. (see color-picture part, page 620) Topography of (a) the Earth, (b) Venus, (c) Mars and (d) the Moon as derived from the topographic models given in Table 8. All images are in a Hammer projection with a central meridian of 0° W. Zero elevation is given by (a) the mean sea level, (b) a sphere of 6051.8 km radius, (c) the gravitational equipotential surface whose average radius at the equator is equal to the mean equatorial radius of 3396 km and (d) a spheroid with an equatorial radius of 1738 km and a flattening of 1/3234.93.

Table 8. Topographic models of the Earth, Venus, Mars and the Moon. Models for the Earth include oceanic bathymetry and landmass topography. Resolution is given as datapoints (pixels) per degree and the resolution of the spherical harmonic representations are given in terms of degree n and order m.

Planet	Name	Resolution	References
Earth	SRTM30_PLUS	120 pxl/°	[03Rab, 05Rod, 97Smi1]
Earth	ETOPO2	30 pxl/°	[06DoC]
Venus	MGN-V-RDRS-5-TOPO-L2-V1.0	1 pxl/°	[92For, 06Sjo, 99Rap]
Mars	MGS-M-MOLA-5-MEGDR-L3-V1.0	128 pxl/°	[03Smi]
Moon	CLEM1-L-LIDAR-5-TOPO-V1.0	4 pxl/°	[96Zub]
Venus	SHTJV360	$n, m = 360$	[06Sjo, 99Rap]
Mars	GTM090AA	$n, m = 90$	[00Neu]
Moon	GLTM-2B	$n, m = 70$	[96Zub, 97Smi2]

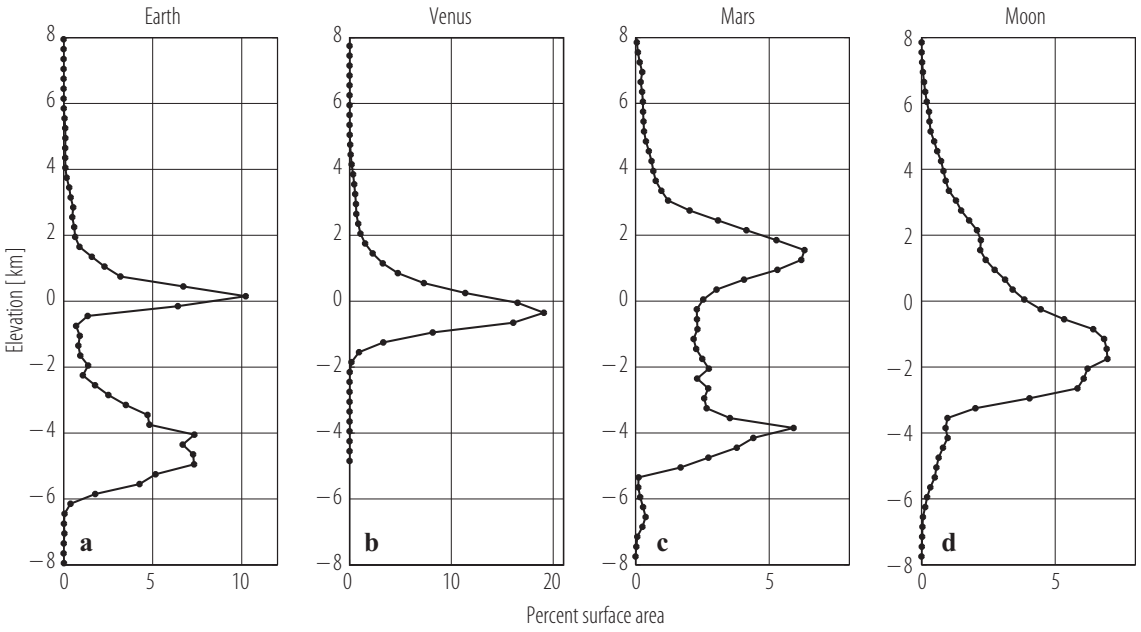

Fig. 5. Hypsometric curves for the Earth, Venus, Mars and the Moon, derived from the topographic models given in Table 8. The bin size for the topographic data is 300 m.

4.2.3.1.5 References for 4.2.3.1

68Mul Muller, P.M., Sjogren, W.L.: Science **161** (1968) 680-684.

92For Ford, P.G., Pettengill, G.H.: J. Geophys. Res. **97** (1992) 13,103-13,114.

94Noz Nozette, S., et al.: Science **266** (1994) 1835-1839.

94Zub Zuber, M.T., et al.: Science **266** (1994) 1839-1843.

95Yod Yoder, C.F.: In: Ahrens, T.J. (ed.), Global Earth Physics: A Handbook of Physical Constants. AGU reference shelf 1, pp. 1-31, Washington D.C., American Geophysical Union (1995).

96Zub Zuber, M.T., Smith, D.E., Neumann, G.A.: CLEM1-L-LIDAR-5-TOPO-V1.0, NASA Planetary Data System (1996).

97Fol Folkner, W.M., et al.: Science **278** (1997) 1749-1752.

97Lem Lemoine, F.G.R., et al.: J. Geophys. Res. **102** (1997) 16,339-16,359.

97Smi1 Smith, W.H.F, Sandwell, D.T.: Science **277** (1997) 1956-1962.

97Smi2 Smith, D.E., et al.: J. Geophys. Res. **102** (1997) 1591-1611.

99Kon1 Konopliv, A.S., Banerdt, W.B., Sjogren, W.L.: Icarus **139** (1999) 3-18.

99Kon2 Konopliv, A.: LP-L-RSS-5-GRAVITY-V1.0, NASA Planetary Data System (1999).

99Rap Rappaport, N.J., Konopliv, A.S., Kucinskas, A.B.: Icarus **139** (1999) 19-31.

00Neu Neumann, G.: MGS-M-MOLA-5-SHADR-V1.0, NASA Planetary Data System (2000).

01Kon Konopliv, A.S., et al.: Icarus **150** (2001) 1-18, doi: 10.1006/icar.2000.6573.

01Neu Neumann, G.A.: Int. Arch. Photogr. Rem. Sens., XXXIV-3/W4 (2001) 73-80.

01Phi Phillips, R.J., et al.: Science **291** (2001) 2587-2591.

01Yua Yuan, D.N., et al.: J. Geophys. Res. **106** (2001) 23,377-23,402, doi: 10.1029/2000JE001302.

03Rab Rabus, P.B., et al.: ISPRS J. Photogrammetry and Remote Sensing **57** (2003) 241-262.

03Smi Smith, D., et al.: MGS-M-MOLA-5-MEGDR-L3-V1.0., NASA Planetary Data System (2003).

05Rod Rodríguez, E., et al.: Technical Report of the Jet Propulsion Laboratory, Pasadena, CA: NASA and CalTech (2005).

05Tyl Tyler, G.L., et al.: MGS-M-RSS-5-SDP-V1.0, NASA Planetary Data System (2005).

06Arc Archinal, B.A., Rosiek, M.R., Kirk, R.L., Redding, B.L.: USGS, Open-File Report, 1367, (2006).

06DoC U.S. Department of Commerce, National Oceanic and Atmospheric Administration, National Geophysical Data Center (2006), http://www.ngdc.noaa.gov/mgg/fliers/06mgg01.html

06Kon Konopliv, A.S., et al.: Icarus **182** (2006) 23-50, doi: 10.1016/j.icarus.2005.12.025.

06Rap Rappaport, N.J., Sjogren, W.L.: MGN-V-RDRS-5-TOPO-L2-V1.0, NASA Planetary Data System (2006).

06Roa Roatsch, T., et al.: Planet. Space Sci. **54** (2006) 1137-1145.

06Sjo Sjogren, W.L.: MGN-V-RSS-5-GRAVITY-L2-V1.0, NASA Planetary Data System (2006).

07Sei Seidelmann, P.K., et al.: Celest. Mech. Dynam. Astron. **98** (2007) 155-180.

07Wie Wieczorek, M.A.: In: Schubert, G., Spohn, T. (eds.): Treatise on Geophysics - Planets and Moons, volume 10, pages 165-206. Elsevier, Amsterdam, 2007.

08För Förste, C., et al.: J. Geodesy **82** (2008) 331-346, doi: 10.1007/s00190-007-0183-8.